energies

MDPI

Article

Implementing Discrete Model of Photovoltaic System on the Embedded Platform for Real-Time Simulation

Aryuanto Soetedjo * and Irrine Budi Sulistiawati

Department of Electrical Engineering, National Institute of Technology (ITN), Malang 65145, Indonesia; irrine@lecturer.itn.ac.id

* Correspondence: aryuanto@lecturer.itn.ac.id

Received: 27 July 2020; Accepted: 25 August 2020; Published: 27 August 2020

Abstract: This paper presents the development of a discrete model of a photovoltaic (PV) system consisting of a PV panel, Maximum Power Point Tracking (MPPT), a dual-axis solar tracker, and a buck converter. The discrete model is implemented on a 32-bit embedded system. The goal of the developed discrete PV model is to provide an efficient way for evaluating several algorithms and models used by the PV system in real-time fashion. The proposed discrete model perfectly matches the continuous and discrete model simulated with MATLAB-SIMULINK. The real-time performance is tested by running the model to simulate the PV system, where the fastest time sampling of 1 ms is achieved by the buck converter model, while the longest time sampling of 100 ms is achieved by the solar tracker model. Moreover, a novel method is proposed to optimize the net energy, which is calculated by subtracting the energy consumed by the tracker from the PV energy generated. The proposed net energy optimization method varies the operation time interval of the solar tracker under high and low solar irradiation conditions. Based on the real-time simulation of the discrete model, our approach increases the net energy by 29.05% compared to the system without the solar tracking and achieves an increase of 1.08% compared to the existing method.

Keywords: photovoltaic; buck converter; MPPT; solar tracker; discrete model; embedded system

1. Introduction

A photovoltaic (PV) system requires several technologies such as Maximum Power Point Tracking (MPPT) and Solar Tracking to improve its energy efficiency. MPPT is a technique that is used to improve the energy efficiency by operating the PV at the maximum power point. This method relies on the non-linear characteristic of the current and voltage relationship of the PV. Basically, the MPPT methods could be divided into two types: conventional methods and intelligent methods. The most popular conventional methods are the Perturb and Observe (P&O) and Incremental Conductance (INC) methods [1]. The most popular intelligent methods are the Fuzzy Logic Controller (FLC) and Artificial Neural Networks (ANN) methods [1].

The P&O method works by perturbing the PV voltage and observing the PV power to achieve the maximum power point [2]. However, the basic algorithm has problems with the response time, oscillation at the maximum power point, and drift under irradiation changes. Therefore, many improved methods have been proposed [3–6]. The authors in [3–5] proposed MPPT methods with a variable step size to deal with the response time and oscillation problems. Several modified algorithms have been proposed in [6,7] to overcome the drift problem.

The INC method was employed to overcome the oscillation problem at the steady state [8–11]. The INC method decreases/increases the PV voltage according to the value of incremental inductance. This method is based on the fact that the derivative of the power with respect to the voltage at the maximum power point is zero. The speed time and accuracy could be improved by introducing

a variable step size, as proposed in [9,10]. The authors in [11] developed a method to switch the algorithm between P&O and INC methods.

FLC-based MPPT methods [12–15] use fuzzy logic to adjust the PV voltage in finding the maximum power point. The FLCs in [12–14] were developed based on the P&O, in the sense that the fuzzy rules were defined based on the P&O algorithm. The FLC inputs are the error and change of error, where the error is the slope of the power–voltage characteristic of the PV. The FLC output is the duty cycle of the DC–DC converter, which is used to adjust the PV voltage. The FLC method in [15] was used to address the drift problem by introducing the ratio of the change in the power to the current power as a fuzzy input.

ANN techniques were used in [14,16] to find the maximum PV power. In [14], the inputs of the ANN are the solar irradiation and PV temperature, while the output is the duty cycle of the DC–DC converter. The ANN is trained using the solar irradiation and PV temperature data to find the optimal voltage. In [16], the ANN is trained using the P&O algorithm, where the ANN inputs are the voltage and current, while the output is the duty cycle of the DC–DC converter.

A solar tracking system moves the PV panel to follow the sun's position, because the sun's energy will be maximally absorbed when the PV panel is perpendicular to the sun's rays. A solar tracking system could be divided into single-axis and dual-axis systems based on their direction of movement [17]. A single-axis solar tracking system tracks the elevation of the sun [18–22], while a dual-axis system tracks both the elevation and azimuth of the sun [23–32]. There are two types of solar tracking systems based on the control strategy: closed-loop and open-loop control [23]. Closed-loop solar tracking systems use sensors (photodiodes) to detect the sun's position [20,24,25,27], while open-loop solar tracking systems do not use sensors; instead, they use an astronomical algorithm to estimate the sun's position [18,22,26,28–31]. The accuracy of the closed-loop solar tracking system is high, but it requires complex sensor hardware and fails to track the sun under the cloudy condition. An open-loop solar tracking system does not require sensors, but the accuracy is lower, and it requires precision real-time clock hardware. To provide an effective solar tracking system, a hybrid open-loop and closed-loop system was proposed in [32]. In this system, closed-loop solar tracking is used to track the sun's elevation, while open-loop solar tracking is used to track the sun's azimuth.

In addition to MPPT and solar tracking, a system to monitor the PV condition is required to increase the efficiency of the PV plant [33]. A PV monitoring system monitors the environmental conditions, electrical parameters of the PV plant, and faulty conditions of the PV. Due to the rapid development of the Internet of Things (IoT) technology, the implementation of IoT-based PV monitoring systems has significantly increased [34–43]. The works in [35,36] focused on the monitoring of the PV temperature. In [35], the PV temperature was monitored to detect the PV efficiency and overheating of the PV module. In [36], the monitoring system was used to monitor the PV temperature located on the rooftop in a hot climate. Low-cost embedded systems equipped with WiFi modules were employed to communicate with a cloud server [35]. The authors in [37] proposed a method to monitor the PV dusty in the harsh environment by analyzing its current–voltage characteristic.

A system to monitor the MPPT algorithm was developed in [38]. This system could be used to monitor MPPT parameters such as the PV voltage, PV current, and duty cycle of the converter in real time via a website. A solar home monitoring system in the rural area using 3G technology was developed in [39], where the electrical and environmental parameters were monitored via a website and mobile application. To cover the wide area and long distance in the PV installations, a long-range (LoRa) technology was proposed in [40]. A PV fault diagnosis system was developed in [41]. It used the extreme learning machine (ELM) to classify the PV faults into four categories: normal, open circuit, short circuit, and partially shaded.

Since the sun is only available for a limited time (morning until afternoon) and PV installation in the rural area or on a rooftop is expensive, it has become common to use a simulation model for research purposes. Simulation models for testing and validating the MPPT techniques were developed in [2–4,6–16]. The works in [5] employed a hardware emulator for testing the MPPT

controller. Simulation models for testing the solar tracking system were developed in [19,23,25,26,29,31]. Unlike the MPPT and the solar tracking systems, most of the PV monitoring systems are developed using real PV systems. Only a few PV monitoring systems use the simulation models, such as the one proposed in [42]. In [42], a virtual PV plant is used in developing the PV monitoring system.

In this paper, we propose a discrete model of a PV system with MPPT and solar tracking. Instead of a continuous model simulated using computer software, our discrete model is implemented on the embedded hardware. To the best of our knowledge, no other system similar to this is available. The main contributions of our work are threefold. First, since the discrete model is implemented on the embedded hardware, a real-time simulation can be performed. Second, our model can easily be integrated with an IoT-based PV monitoring system for the real-time monitoring applications. Third, using our proposed system, we may evaluate the solar tracker operation time interval to achieve the optimal energy produced by the PV system. This last contribution deals with energy optimization in the solar tracking system in relation to the energy consumption of the solar tracker operation.

The rest of the paper is organized as follows. Section 2 presents the proposed system consisting of our proposed discrete model of the PV system. The experimental results and discussion are described in Section 3. The conclusion is covered in Section 4.

2. Proposed System

2.1. System Configuration

The configuration of the proposed system is depicted in Figure 1. The proposed discrete PV model (hereinafter called as the PV Dis-Mod) consists of five main components: (a) Solar model; (b) PV panel model; (c) Solar tracker model; (d) Buck converter model; and (e) MPPT. The solar model is used to generate the effective solar irradiance (*Geff*) directing to the PV panel. The *Geff* is the solar irradiation which is perpendicular to the PV panel. It is affected by the solar position and the pan and tilt of the PV panel. In the solar model, the solar azimuth and elevation are calculated using an astronomy algorithm [44–47] that utilizes the latitude and longitude of the PV site. The solar azimuth and elevation are fed to the solar tracking system for determining the PV pan and tilt.

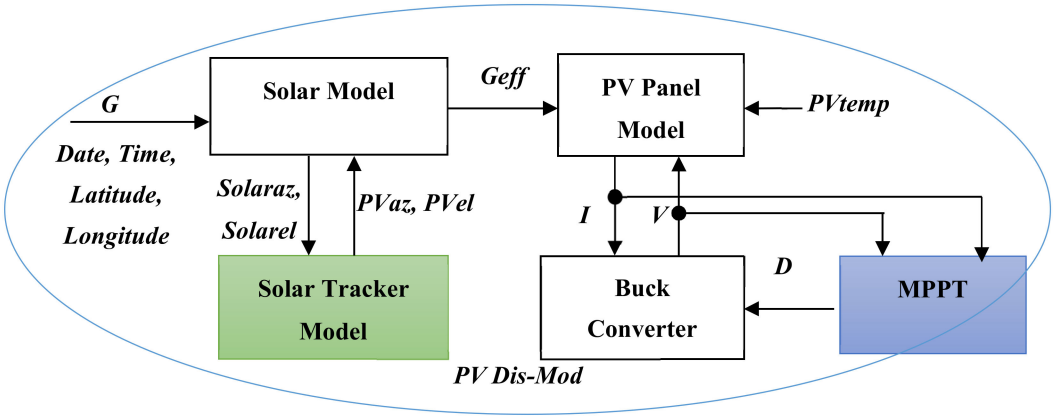

Figure 1. Configuration of the proposed discrete photovoltaic (PV) model. *G*: solar irradiation; *Geff*: effective solar irradiation; *PVtemp*: PV temperature; *Solaraz*: solar azimuth; *Solarel*: solar elevation; *PVaz*: PV panel azimuth; *PVel*: PV panel elevation; *V*: PV voltage; *I*: PV current; *D*: duty cycle of DC-DC converter; PV Dis-Mod: Discrete PVmodel.

The PV panel model is a mathematical model of the PV proposed in [48–50]. In the model, the PV voltage and ambient temperature are considered to be the inputs, while the output is the PV current. The PV panel model is connected to the buck converter model and the MPPT controller. The solar tracker model is a discrete model of the dual-axis solar tracker proposed in [31]. This tracker employs two DC motors to track the solar azimuth and elevation. Proportional Integral Derivative (PID)

controllers are used to control the position of the motors. The solar tracker model is used to calculate the pan (azimuth) and tilt (elevation) of the PV panel so that they are perpendicular to the solar azimuth and elevation. The buck converter model adopts the model proposed in [2,31,51]. The buck converter is driven by a pulse width modulation (PWM) signal generated by the MPPT controller. The converter is used to change the PV voltage and current according to the MPPT algorithm, in the case of the P&O technique.

2.2. PV Panel Model

The PV panel model [50] is illustrated in Figure 2, which consists of one diode and a photocurrent source. The relationship between the voltage and current can be derived from the following equations [48,50]:

$$I = N_p I_{PH} - N_p I_S \left[e^{\frac{q(V/N_s)}{kT_C A}} - 1 \right] \quad (1)$$

$$I_{PH} = [I_{SC} + K_I(T_C - T_R)]G \quad (2)$$

$$I_S = I_{RS} \left(\frac{T_C}{T_R} \right)^3 e^{\left[\frac{qE_G}{kA} \left(\frac{1}{T_R} - \frac{1}{T_C} \right) \right]} \quad (3)$$

$$I_{RS} = \frac{I_{SC}}{e^{\frac{qV_{OC}}{N_s k A T_C}} - 1} \quad (4)$$

where I is the PV current, V is the PV voltage, I_{PH} is the photocurrent, I_S is the cell saturation of the dark current, q is an electron charge ($q = 1.6 \times 10^{-19}$ C), k is Boltzmann's constant ($k = 1.38 \times 10^{-23}$ J/K), T_C is the cell's temperature, A is an ideal factor ($A = 1.2$), I_{SC} is the cell's short circuit current at the temperature of 25 °C and solar irradiation of 1000 W/m^2 ($I_{SC} = 3.25$ A), K_I is the temperature coefficient of the cell's short circuit current ($K_I = 0.003$), T_R is the cell's reference temperature ($T_R = 298.15$ K), G is the solar irradiation (in kW/m^2), I_{RS} is the reverse saturation current, E_G is the band gap energy ($E_G = 1.1$ eV), V_{OC} is the open circuit voltage ($V_{OC} = 0.6$ V), N_p is the number of cells connected in parallel ($N_p = 1$), and N_s is the number of cells connected in series ($N_s = 36$).

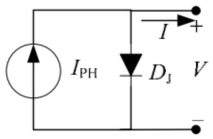

Figure 2. PV panel model [50].

2.3. Solar Posistion Model

The solar position is computed using the algorithm proposed in [31,44–47]. The algorithm to find the solar azimuth and elevation is described using the following equations:

$$SIDTIME = GMST0 + UTH + Longi/15 \quad (5)$$

$$HA = (15\ SIDTIME - RA) \quad (6)$$

$$xc = \cos(HA(\pi/180))\cos(Decl(\pi/180)) \quad (7)$$

$$yc = \sin(HA(\pi/180))\cos(Decl(\pi/180)) \quad (8)$$

$$zc = \sin(Decl(\pi/180)) \quad (9)$$

$$xhor = (xc \cos((90\text{-}Lat)(\pi/180))) - (zc \sin((90\text{-}Lat)(\pi/180))) \quad (10)$$

$$yhor = yc \quad (11)$$

$$zhor = (xc \sin((90\text{-}Lat)(\pi/180))) + (zc \cos((90\text{-}Lat)(\pi/180))) \quad (12)$$

$$Az = \tan^{-1}(yhor/xhor)(180/\pi) + 180 \quad (13)$$

$$El = \sin^{-1}(zhor)(180/\pi) \quad (14)$$

where *SIDTIME* is the local sidereal time, *GMST*0 is the Greenwich mean sidereal time, UTH is the Greenwich time, *Longi* is the longitude of the PV site, *HA* is the hour angle, *RA* is the right ascension, (*xc*, *yc*, *zc*) are the rectangular coordinate system, *Decl* is the declination, (*xhor*, *yhor*, *zhor*) are the rotation of (*xc*, *yc*, *zc*) along the east–west axis, *Lat* is the latitude of the PV site, *Az* is the solar azimuth, and *El* is the solar elevation. The formulas to calculate *RA*, *Decl*, and *GMST0* can be found in [31,44–47].

The effective solar irradiation (*Geff* in Figure 1) is obtained using the following formula:

$$Geff = Gind(\cos(El)\sin(\beta)\cos(\theta - Az) + \sin(El)\cos(\beta)) \quad (15)$$

where *Gind* is the incident solar irradiation, θ is the PV panel's azimuth angle, and β is the PV panel's tilt angle.

2.4. Solar Tracker Model

The continuous model of the solar tracker is depicted in Figure 3. The azimuth tracker and elevation tracker use the same model. In the figure, the right block represents the DC motor, while the left one is the PID controller. In this research, the DC motor's parameters are adopted from [29], where k_e is the motor constant ($k_e = 0.03103$), L_a is the armature inductance ($L_a = 0.00866$ H), f is the damping coefficient ($f = 0.000025$ Nms/rad), R_a is the armature resistance ($R_a = 18.2214\ \Omega$), and J is the moment of inertia ($J = 0.000090$ kgm^2). The parameters of the PID controller are the proportional gain ($K_p = 0.0805$), integral gain ($K_i = 0.0011$), and derivative gain ($K_d = 0.0635$).

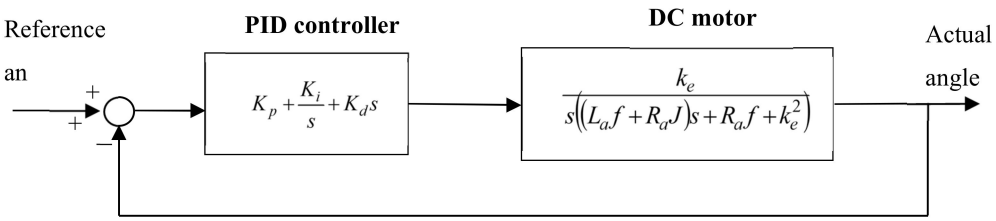

Figure 3. Solar tracker model [31].

The closed loop transfer function of the actual angle ($\theta_a(s)$) to the reference angle ($\theta_r(s)$) is defined below:

$$\frac{\theta_a(s)}{\theta_r(s)} = \frac{0.00197s^2 + 0.002498s + 0.00003413}{0.0016s^3 + 0.00337s^2 + 0.002498s + 0.00003413}. \quad (16)$$

The discrete model of the solar tracker is obtained by converting the transfer function in the *s*-domain, Equation (16), to the *z*-domain. In this research, the conversion is performed using the MATLAB script, and the discrete transfer function is given below (the time sampling is 100 ms):

$$\frac{\theta_a(z)}{\theta_r(z)} = \frac{0.118z^2 - 0.222z + 0.104}{z^3 - 2.796z^2 + 2.606z + 0.8101} \quad (17)$$

where $\theta_a(z)$ and $\theta_r(z)$ are the actual angle and reference angle in the *z*-domain, respectively.

In order to be implemented on an embedded system, the transfer function in Equation (17) is converted to the following difference equation:

$$y[k] = 2.796y[k-1] - 2.606y[k-2] + 0.810y[k-3] + 0.118x[k-1] - 0.222x[k-2] + 0.104x[k-3] \quad (18)$$

where $y[k]$, $y[k-1]$, $y[k-2]$, and $y[k-3]$ are the actual angles at step-k, step-$(k-1)$, step-$(k-2)$, and step-$(k-3)$, respectively, $x[k-1]$, $x[k-2]$, and $x[k-3]$ are the reference angles at step-$(k-1)$, step-$(k-2)$, and step-$(k-3)$ respectively, and step-n is the current step.

2.5. MPPT

The P&O, the most popular MPPT technique, is adopted in this research. The algorithm is depicted in Figure 4. As shown in the figure, it first calculates the PV power at step-k ($P[k]$). Then, the change in power ($\Delta P[k]$) and change in voltage ($\Delta V[k]$) are calculated using the following formulas:

$$P[k] = V[k]\, I[k] \tag{19}$$

$$\Delta P[k] = P[k] - P[k-1] \tag{20}$$

$$\Delta V[k] = V[k] - V[k-1] \tag{21}$$

where $V[k]$ and $I[k]$ are the PV voltage and current at step-k respectively, and $P[k-1]$ and $V[k-1]$ are the power and voltage at step-$(k-1)$, respectively.

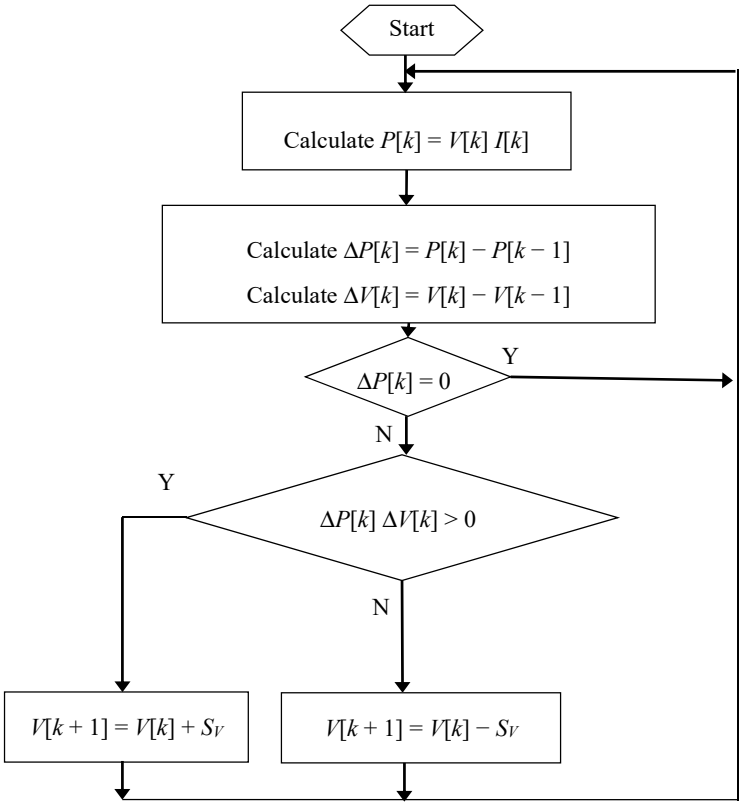

Figure 4. Flowchart of Perturb and Observe (P&O) algorithm [4].

Then, the algorithm checks the value of $\Delta P[k]$ and ($\Delta P[k]\ \Delta V[k]$). Based on these values, the next action is performed as follows.

- If $\Delta P[k] = 0$, then the maximum power point is reached.
- If ($\Delta P[k]\ \Delta V[k] > 0$), then the voltage at the next step should be increased ($V[k+1] = V[k] + S_V$), where S_V is the step size of the perturbation voltage,
- If ($\Delta P[k]\ \Delta V[k] \leq 0$), then the voltage at the next step should be decreased ($V[k+1] = V[k] - S_V$), where S_V is the step size of the perturbation voltage.

2.6. Buck Converter Model

The electrical circuit of a buck converter model is depicted in Figure 5 [2]. The model consists of a power switch device (*S*), a freewheeling diode (*FD*), an inductor (*Ind*), and a capacitor (*Cap*). The relationship between the voltage input (v_{in}) and the voltage output (v_{out}) is determined by the following formulas, where the model is expressed in the discrete form:

$$i_L[k] = \frac{i_S[k] - Q_r f_s}{D + t_r f_s} \tag{22}$$

$$di_L[k] = \frac{i_L[k] - i_L[k-1]}{T_s} \tag{23}$$

$$v_C[k] = \frac{T_s}{C}\sum_{j=0}^{k} i_C[j] \tag{24}$$

$$v_{in}[k] = \frac{(Ldi_L[k]) + (i_L[k](R_{on} + R_L)) + v_C[k] + ((i_L[k] - i_{load}[k])esr)}{D} \tag{25}$$

$$i_C[k] = i_L[k] - i_{load}[k] \tag{26}$$

$$v_{out}[k] = v_C[k] + (i_L[k] - i_{load}[k]esr) \tag{27}$$

where i_L is the inductor current, i_S is the input current, Q_r is the diode recovered charge ($Q_r = 100 \times 10^{-9}$ C), f_s is the switching frequency ($f_s = 40$ kHz), D is the duty cycle, t_r is the diode reverse recovery time ($t_r = 50 \times 10^{-9}$ s), T_s is the time sampling ($T_s = 1$ ms), v_C is the capacitor voltage, C is the capacitance of the capacitor ($C = 4.7$ mF), i_C is the capacitor current, L is the inductance of the inductor ($L = 100$ µH), R_{on} is the resistance of the power switch device at the ON state ($R_{on} = 0.05$ Ω), R_L is the resistance of the inductor ($R_L = 0.1$ Ω), i_{load} is the load current, and esr is the equivalent series resistance of the capacitor ($esr = 0.05$ Ω).

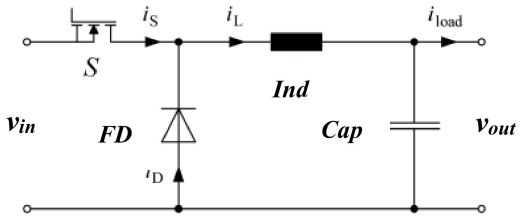

Figure 5. Buck converter model [2].

2.7. Optimization of Solar Tracker Energy

Our proposed solar tracker employs two DC motors to track the solar azimuth and elevation. Since the motors consume energy during their operation, a strategy is required to optimize the operation time of the motors. In [30], the elevation tracker moves up every 10° (19 s), moves down every 10° (14 s), and the azimuth tracker moves every 1° (1.1 s). In [32], the elevation and azimuth motors are operated every 15° (1 h).

In this research, we evaluate the impact of tracker operation time on the net energy of the PV system, where the net energy is defined by subtracting the energy consumed by the tracker from the energy generated by the PV. Two tracker operation strategies are compared. First, a fixed time interval is used, where the azimuth and elevation trackers move every 1 min. Second, a variable time interval is used, where the time intervals for operating the trackers are varied depending on the time of day as given in Table 1. The latter strategy is based on the fact that the energy consumed by the solar tracker depends only on the time interval, while the energy produced by the PV depends on both the time interval and the solar irradiation. Thus, by setting a longer time interval at noon (with high

solar irradiation), the tracker energy is greatly reduced, whereas the high solar irradiation causes the PV power to be high, and prolonging the time interval of the tracker only slightly decreases the PV energy. Therefore, it results in a more efficient net energy. It is worth noting here that the selection of the interval values given in Table 1 is based on the observation of the experimental results that will be discussed in the next section.

Table 1. Time interval of tracker operation.

No	Time of the Day (h)	Time Interval of Tracker Operation	
		Azimuth Tracker (min)	Elevation Tracker (min)
1	07:00–09:59	10	10
2	10:00–13:59	20	20
3	14:00–17:59	10	10

3. Experimental Results and Discussion

3.1. Model Verification

3.1.1. PV Panel Model Verification

The PV panel model verification is conducted by comparing the proposed model, which is implemented on the embedded system (Wemos [52], a 32-bit microcontroller) and a model simulated using MATLAB/Simulink. Since the MATLAB model is a common approach to simulate the PV panel model expressed in Equations (1)–(4), it is reasonable to use the Simulink model as the reference model for the verification of our proposed model.

In the experiments, the relationship between the PV voltage and current is evaluated under the three different conditions listed in Table 2. The evaluation results are illustrated in Figure 6, where the I–V curves obtained by the MATLAB and Wemos are plotted for each condition. In the figure, the rhombus, square, and triangle markers represent the model simulated by MATLAB using the solar irradiation and the PV temperature of (1000 W/m^2, 25 °C), (700 W/m^2, 25 °C), and (700 W/m^2, 25 °C) respectively. The cross sign, plus sign, and circle markers represent the model implemented on the Wemos using the solar irradiation and PV temperature of (1000 W/m^2, 25 °C), (700 W/m^2, 25 °C), and (700 W/m^2, 25 °C), respectively. The figure clearly shows that for each condition, both models are almost matched perfectly. The slight discrepancies are caused by the difference in the precision formats of the floating-point numbers, where MATLAB uses 64-bits and Wemos uses 32-bits.

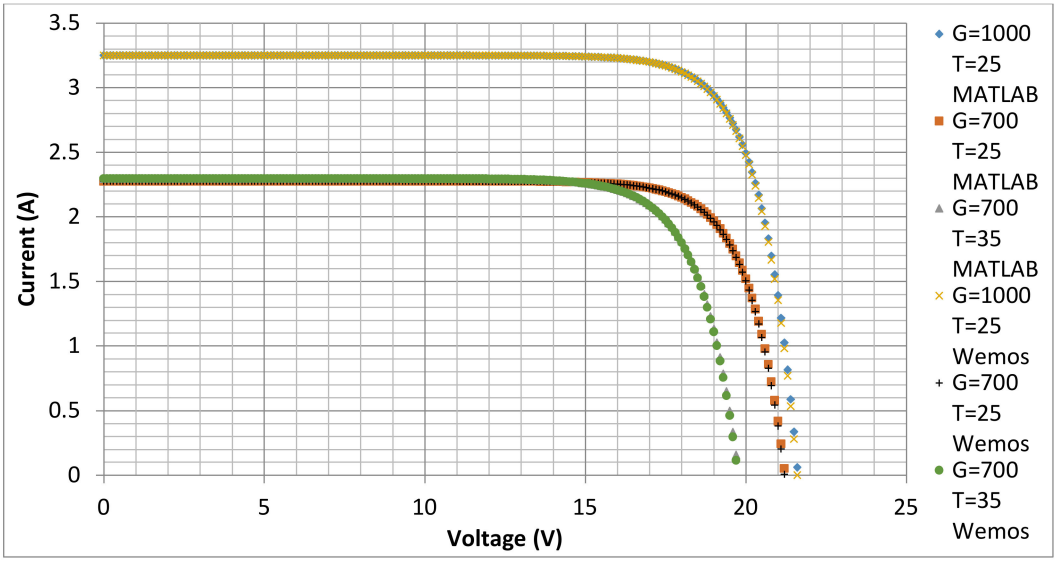

Figure 6. PV current and voltage characteristic of models.

Table 2. Environmental parameters for PV panel model evaluation.

No.	Solar Irradiation (W/m^2)	PV Temperature (°C)
1	1000	25
2	700	25
3	700	35

3.1.2. Solar Tracker Response Time

As discussed previously, the closed-loop transfer function of the solar tracker is modeled as a third-order system, where the continuous transfer function, discrete transfer function, and difference equation are defined in Equations (16)–(18), respectively. The response times of the unit steps are plotted in Figure 7, where the line represents the continuous model simulated using MATLAB, the square marker represents the discrete model simulated using MATLAB, and the triangle marker represents the discrete model implemented on Wemos. The evaluation of response time is important when operating the tracker to follow the solar movement, as discussed below.

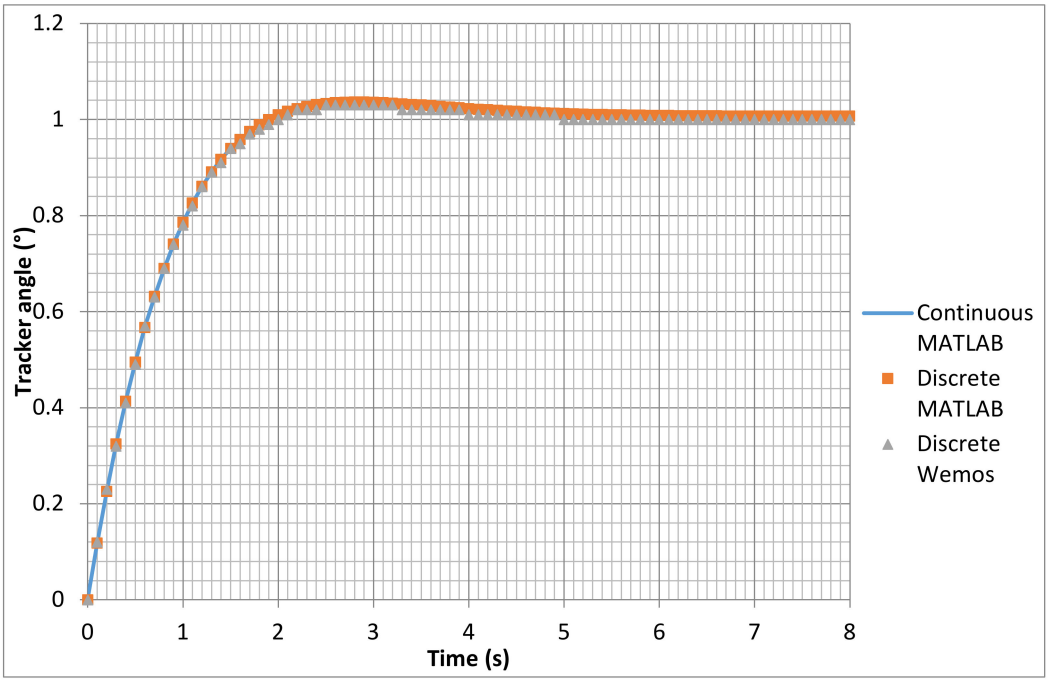

Figure 7. Response times of solar tracker models.

In our proposed system, the time interval of the solar tracker operation is given in Table 1, where the fastest time is 10 min. However, as described previously, we also make a comparison to the solar tracker with a time interval of 1 min. It suggests that the response time of the solar tracker should be less than 1 min. From Figure 7, it is obtained that the settling time of our solar tracker model is approximately 5 s. Thus, the solar tracker model fulfills this requirement.

By comparing the three models in Figure 7, we may conclude that the discrete models using a time sampling of 100 ms are adequate to represent the continuous model, in the sense that the response times of the unit steps are almost matched perfectly. Moreover, our proposed discrete model implemented on Wemos only shows a slight discrepancy compared to the one simulated using MATLAB. Similar to the PV model, this discrepancy is caused by the difference in the precision format of the floating-point numbers.

3.1.3. Buck Converter Response Time

The buck converter is one of the main components in the PV system and is employed by the MPPT to control the PV voltage. Thus, the response time of the buck converter should be fast enough to accommodate the solar irradiation changes and MPPT algorithm. In this work, as discussed in the previous section, the time sampling of the buck converter model expressed by Equations (22)–(27) is set to 1 ms. The response times of the buck converter models are plotted in Figure 8, where the line denotes the continuous model simulated by MATLAB, the square marker denotes the discrete model simulated by MATLAB, and the triangle marker denotes the proposed discrete model implemented on Wemos.

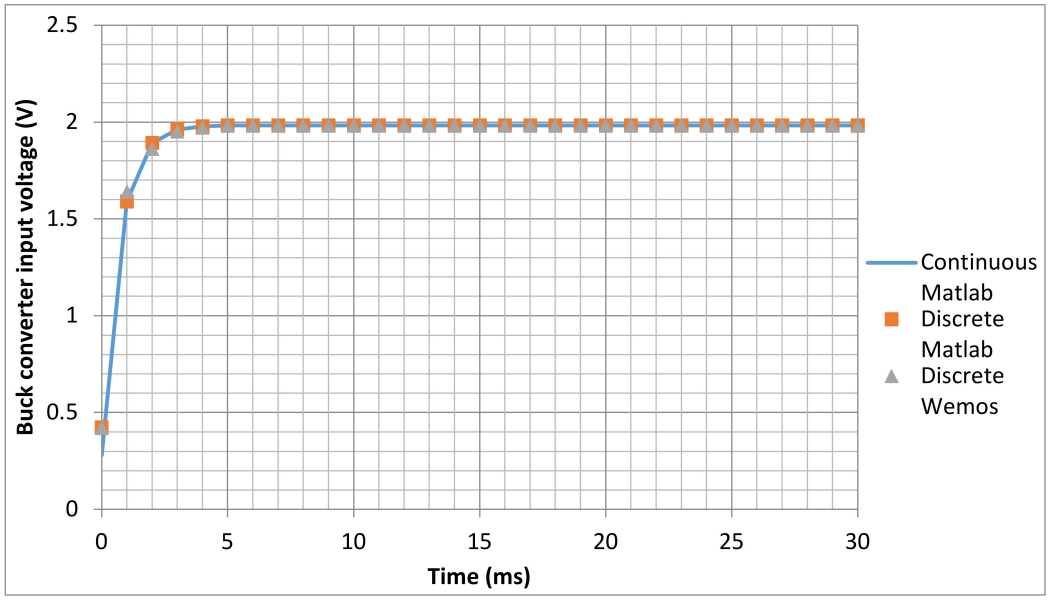

Figure 8. Response times of buck converter models.

From Figure 8, it is obtained that the response times of the three models are almost matched perfectly. Therefore, the proposed discrete model implemented on Wemos is adequate to represent the buck converter model. The settling time of the buck converter is approximately 5 ms, and it is fast enough to be used in the experiments. Similar to the PV model and the solar tracker model, the discrete model implemented on Wemos shows a slight discrepancy with the one simulated by MATLAB due to the difference in the precision format of the floating-point numbers.

3.1.4. MPPT Evaluation

To evaluate the MPPT algorithm (P&O), we run the discrete PV model without the solar tracker on Wemos. The MPPT parameters and environmental conditions are given in Table 3. The response time of the MPPT algorithm is plotted in Figure 9, where the grey line denotes the PV power, and the blue line denotes the solar irradiation. As shown in the figure, it is obtained that for a high solar irradiation (1000 W/m^2) and an initial duty cycle of 0.5, the maximum power point is achieved at approximately 200 ms. From the experiment, it is found that the maximum power is 56 W and the duty cycle in the steady state is 0.48. This maximum power complies with the observation of the PV voltage–current characteristic shown in Figure 6.

Table 3. Maximum Power Point Tracking (MPPT) parameters and environmental conditions.

Time (ms)	Solar Irradiation (W/m^2)	PV Temperature (°C)	MPPT Parameters
0–5000	1000	25	Time sampling = 10 ms, Step size
5001–10,000	300	25	(S_V) = 0.001, Initial duty cycle = 0.5

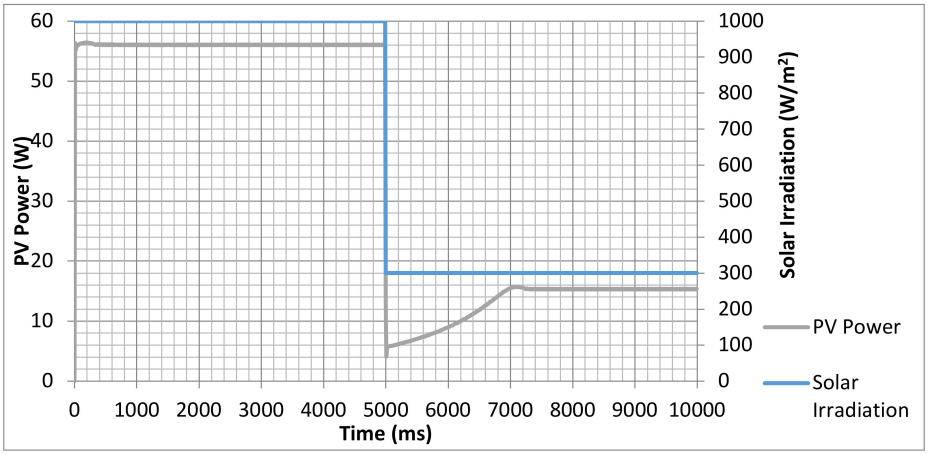

Figure 9. Response time of MPPT algorithm.

From Figure 9, it is obtained that for a low solar irradiation (300 W/m^2) and an initial duty cycle of 0.48 (at a time of 5000 ms), the MPPT algorithm requires approximately 2000 ms to achieve the maximum power. From the experiment, it is found that the maximum power is approximately 15.5 W and the duty cycle in the steady state is 0.27.

3.2. Real-Time Simulation

As described previously, the main objective of our discrete model is to simulate the PV system model in real time. The real-time simulation is conducted by running the discrete model implemented on Wemos (PV Dis-Mod) using predefined environmental data. The environmental data consisted of the solar irradiation and PV temperature, where their profiles during a day from 07:00 to 17:59 h are shown in Figure 10. Both the solar irradiation and PV temperature change every hour. The PV model site is at Malang city, Indonesia, with a longitude of 112.621391° E and latitude of 7.983908° S.

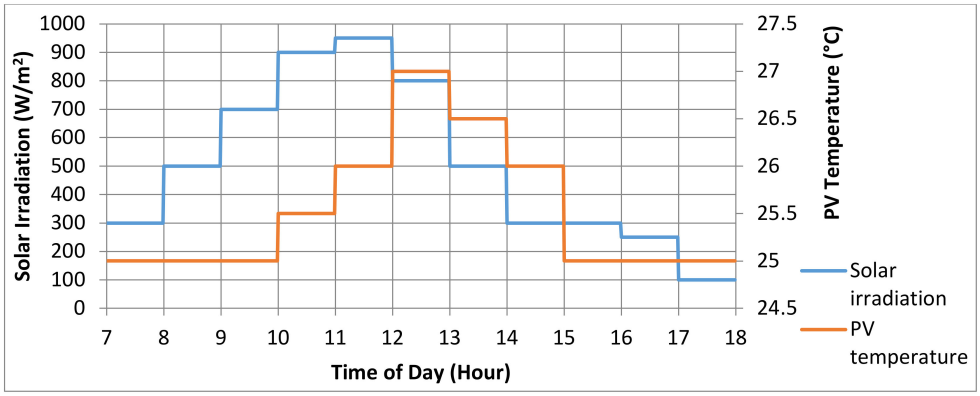

Figure 10. Profiles of solar irradiation and PV temperature.

To provide an efficient time during the evaluation process, a real 1 min time is simulated in 5 s on Wemos. Thus, a real 1 h time is simulated in 5 min. Using this method, evaluating the PV model from 07:00 h to 17:59 h only requires 55 min. Therefore, it is suitable to test several algorithms and models for research purposes in the laboratory.

In the experiments, we compare four PV Dis-Mod models, namely (a) PV Dis-Mod without solar tracking (called as Mod_NT); (b) PV Dis-Mod having both azimuth and elevation trackers operate every 1 min (called as Mod_TR_1m1m); (c) PV Dis-Mod having an azimuth tracker operate every 15 min and an elevation tracker operate every 30 min (called as Mod_TR_15m30m); and (d) PV Dis-Mod having the variation of the solar tracker interval time as given in Table 1 (called Mod_TR_Var). It is noted here that the Mod_TR_1m1m is used to represent the fastest time interval that can be applied to our

model, as explained in the following. From Figure 9, it is obtained that the longest response time of the MPPT algorithm is approximately 2 s. Since the fastest time interval of the solar tracker is 1 min, it will be simulated in 5 s on Wemos, which is longer than 2 s. Thus, it applies to our proposed model. Mod_TR_15m30m is used to represent the existing method proposed in [30] with some adjustments to our application, where the solar tracker takes 15 min to move 1^0 in the azimuth position, and it takes 30 min to move 10^0 in the elevation position.

3.2.1. Effective Solar Irradiation on PV Model

As given in Equation (15), the effective solar irradiation depends on the solar position and solar tracker. Since the operation times of the solar trackers for the four PV Dis-Mod models are different, the profiles of the effective solar irradiation on each PV model will be different as depicted in Figure 11, where Figure 11a shows the profiles from 07:00 to 17:59 h and Figure 11b shows closer look profiles from 10:00 to 12:00 h. The blue, orange, grey, and yellow lines denote Mod_NT, Mod_TR_1m1m, Mod_TR_15m30m, and Mod_TR_Var, respectively.

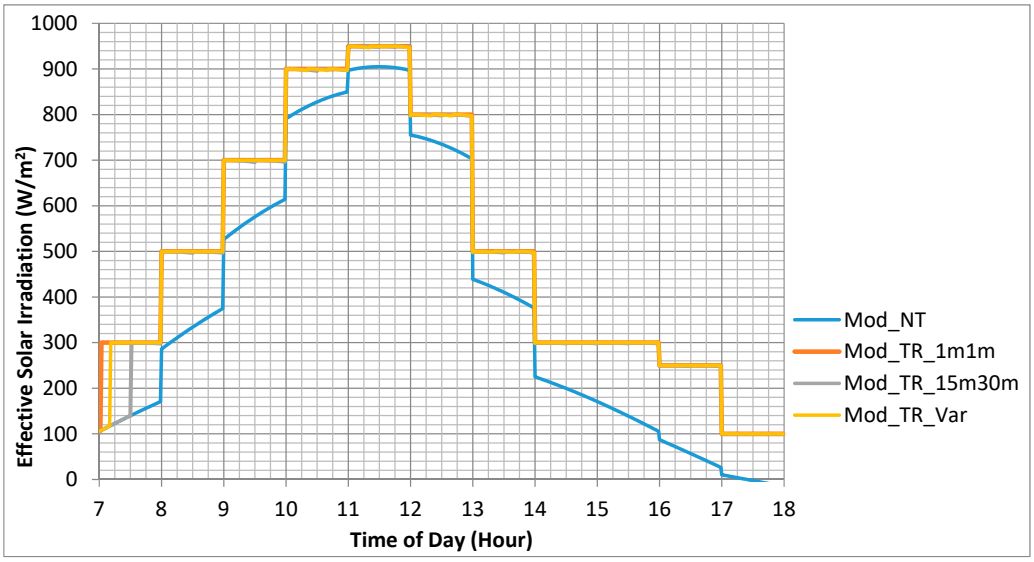

(**a**)

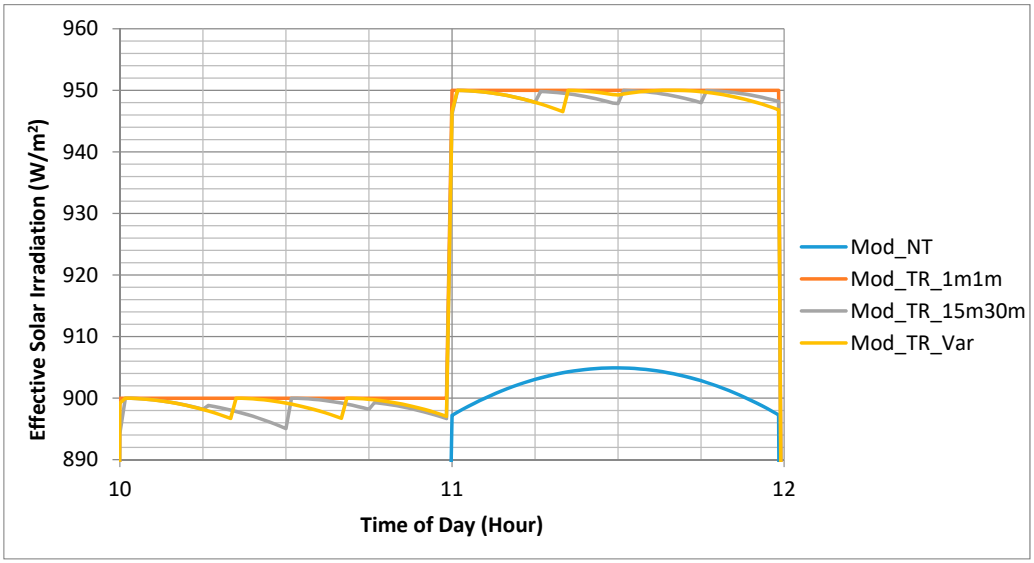

(**b**)

Figure 11. Effective solar irradiation values for PV models: (**a**) Profiles from 07:00 to 17:59 h; (**b**) Closer look profiles from 10:00 to 12:00 h.

As shown in Figure 11a, since there is no solar tracker, the effective solar irradiation on Mod_NT is the lowest one compared to the others. The profiles of the effective solar irradiation for Mod_TR_1m1m, Mod_TR_15m30m, and Mod_TR_Var are almost the same. However, from the closer look profiles shown in Figure 11b, we may see their differences. It is clearly shown that the flat profile (highest value) of the effective solar irradiation is achieved by Mod_TR_1m1m. In the cases of Mod_TR_15m30m and Mod_TR_Var, since the trackers operate in the time interval of 15 min or 20 min, the solar irradiation is the same with the flat one (highest value) at the beginning of the interval and then decreases until the next interval. The decrease in the solar irradiation is caused by the fact that the solar tracker only moves at the beginning and then stops until the next interval.

3.2.2. PV Power

The profiles of the PV power generated by the PV models are depicted in Figure 12, where Figure 12a shows the profiles from 07:00 to 17:59 h, and Figure 12b shows the closer look profiles from 11:00 to 13:00 h. In the figures, the blue, orange, grey, and yellow lines represent Mod_NT, Mod_TR_1m1m, Mod_TR_15m30m, and Mod_TR_Var, respectively.

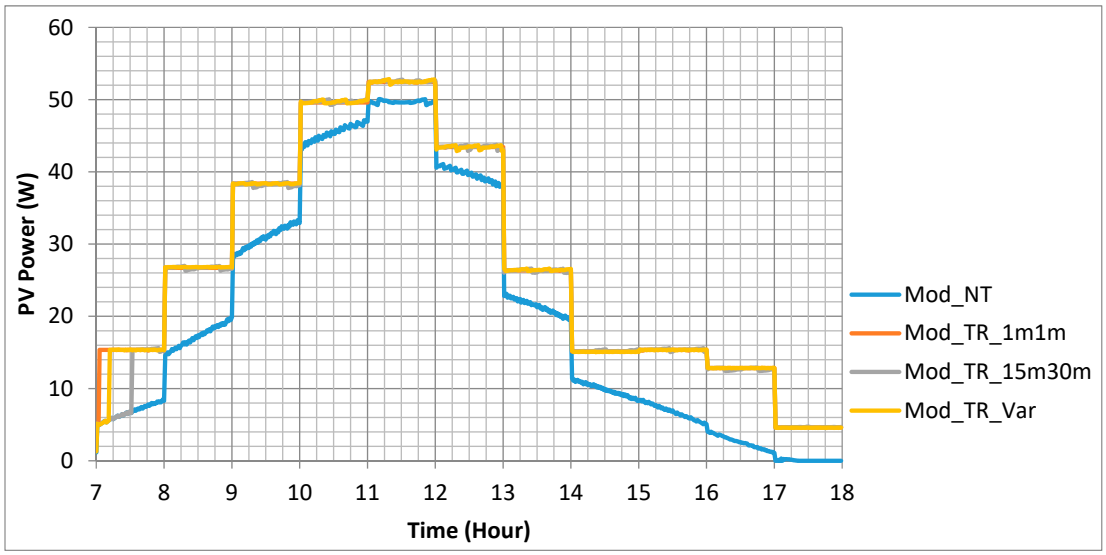

(**a**)

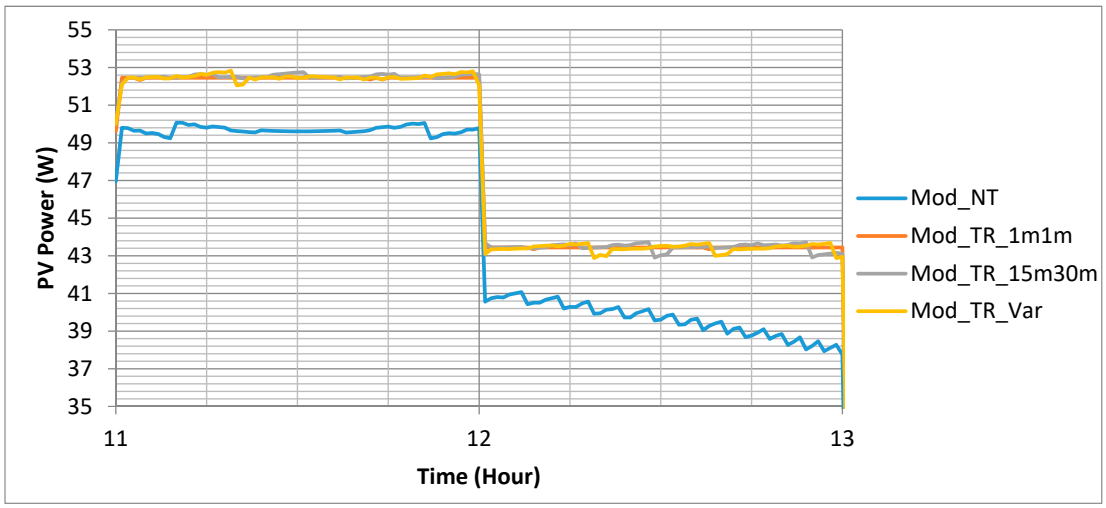

(**b**)

Figure 12. PV power generated by PV models: (**a**) Profiles from 07:00 to 17:59 h; (**b**) Closer look profiles from 11:00 to 13:00 h.

As expected, the profiles of the PV power shown in Figure 12 follow the profiles of the effective solar irradiation shown in Figure 11. The highest PV power is achieved by Mod_TR_1m1m, while the lowest one is achieved by Mod_NT. As shown in the closer look profiles (Figure 12b), the profiles of the PV power generated by Mod_TR_15m30m and Mod_TR_Var fluctuate according to their solar tracker time intervals.

3.2.3. PV Energy

The profiles of the PV energy values are depicted in Figure 13, where Figure 13a shows the profiles from 07:00 to 17:59 h, and Figure 13b shows closer look profiles from 15:00 to 17:59 h. In the figures, the blue, orange, grey, and yellow lines represent Mod_NT, Mod_TR_1m1m, Mod_TR_15m30m, and Mod_TR_Var, respectively.

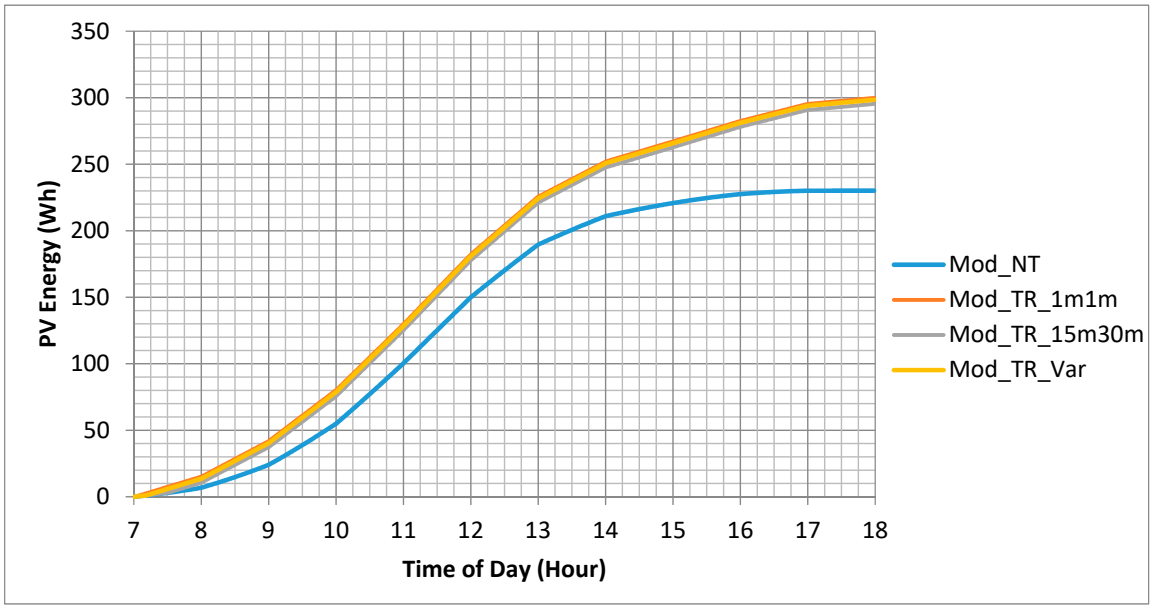

(**a**)

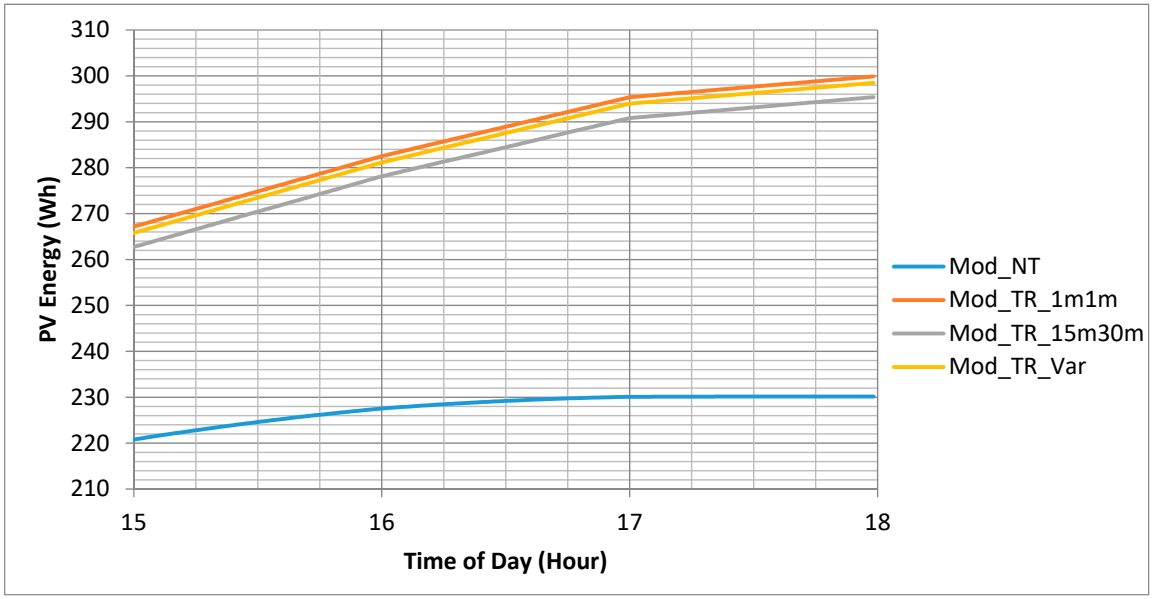

(**b**)

Figure 13. PV energy generated by PV models: (**a**) Profiles from 07:00 to 17:59 h; (**b**) Closer look profiles from 15:00 to 17:59 h.

From the figure, it is obtained that the highest to lowest PV energies are achieved by Mod_TR_1m1m, Mod_TR_Var, Mod_TR_15m30m, and Mod_NT. This result could be understood from the fact that by operating the solar tracker in the faster time interval, the effective solar irradiation on the PV panel will be higher, and as consequence, the PV power will be higher. Thus, the generated PV energy will be higher. By observing closer look profiles on Figure 13b, we can see that the PV energy of our proposed method (Mod_TR_Var) is higher than that of the existing method [30] (Mod_TR_15m30m) and slightly lower than that of Mod_TR_1m1m.

3.2.4. Net Energy

The profiles of the energy consumed by the solar tracker from 07:00 to 17:59 h are depicted in Figure 14, where the red, green, and purple lines represent Mod_TR_1m1m, Mod_TR_15m30m, and Mod_TR_Var, respectively. From the figure, it is clearly shown that the solar tracker having the fastest time interval (Mod_TR_1m1m) consumes the highest energy. It is worth noting that our proposed tracker (Mod_TR_Var) consumes much less energy than Mod_TR_1m1m. Moreover, the energy consumed by Mod_TR_Var is slightly greater than that consumed by Mod_TR_15m30m.

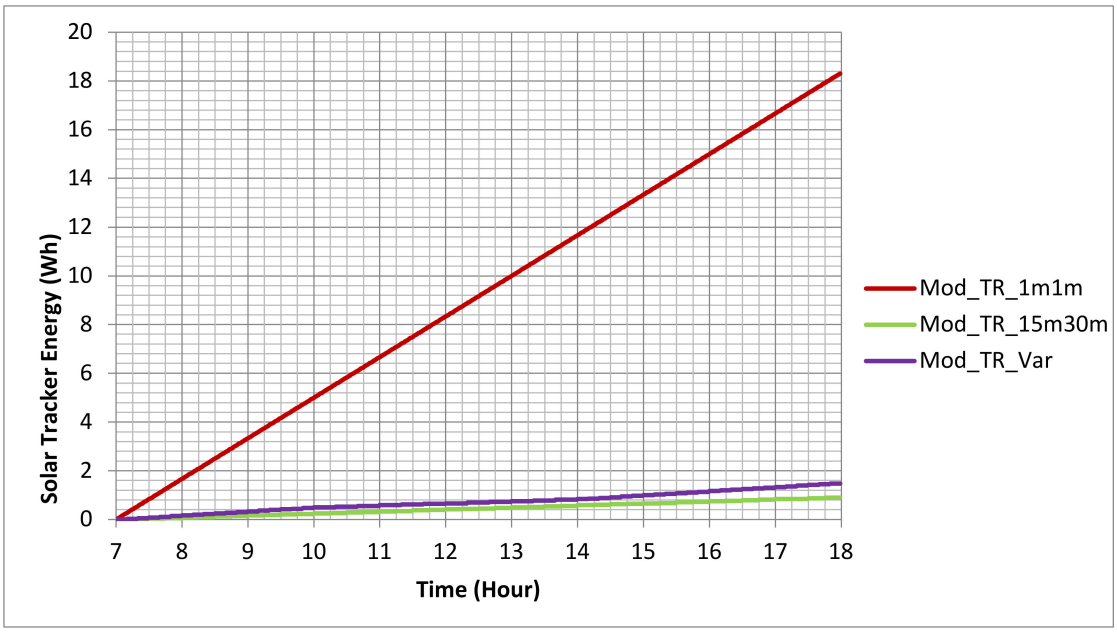

Figure 14. Energy consumed by solar tracker.

The profiles of the net energy values of the models are depicted in Figure 15. The profiles from 07:00 to 17:58 h are depicted in Figure 15a, while closer look profiles from 16:00 to 17:59 h are depicted in Figure 15b. In the figure, the blue, red, green, and purple lines represent Mod_NT, Mod_TR_1m1m, Mod_TR_15m30m, and Mod_TR_Var, respectively.

From the figure, it is obtained that the highest to lowest net energy values are achieved by Mod_TR_Var, Mod_TR_15m30m, Mod_TR_1m1m, and Mod_NT. As listed in Table 4, the net energy of Mod_TR_Var is 29.05% greater than that of Mod_NT. The increase is 1.08% and 6.07% greater than the increases achieved by Mod_TR_15m30m and Mod_TR_1m1m, respectively. The results show that our proposed approach (Mod_TR_Var) provides an efficient way to provide the highest net energy compared to the existing methods. In contrast, although the method with the fastest time interval (Mod_TR_1m1m) generates the greatest PV energy, its solar tracker consumes the most energy. Thus, the net energy is low.

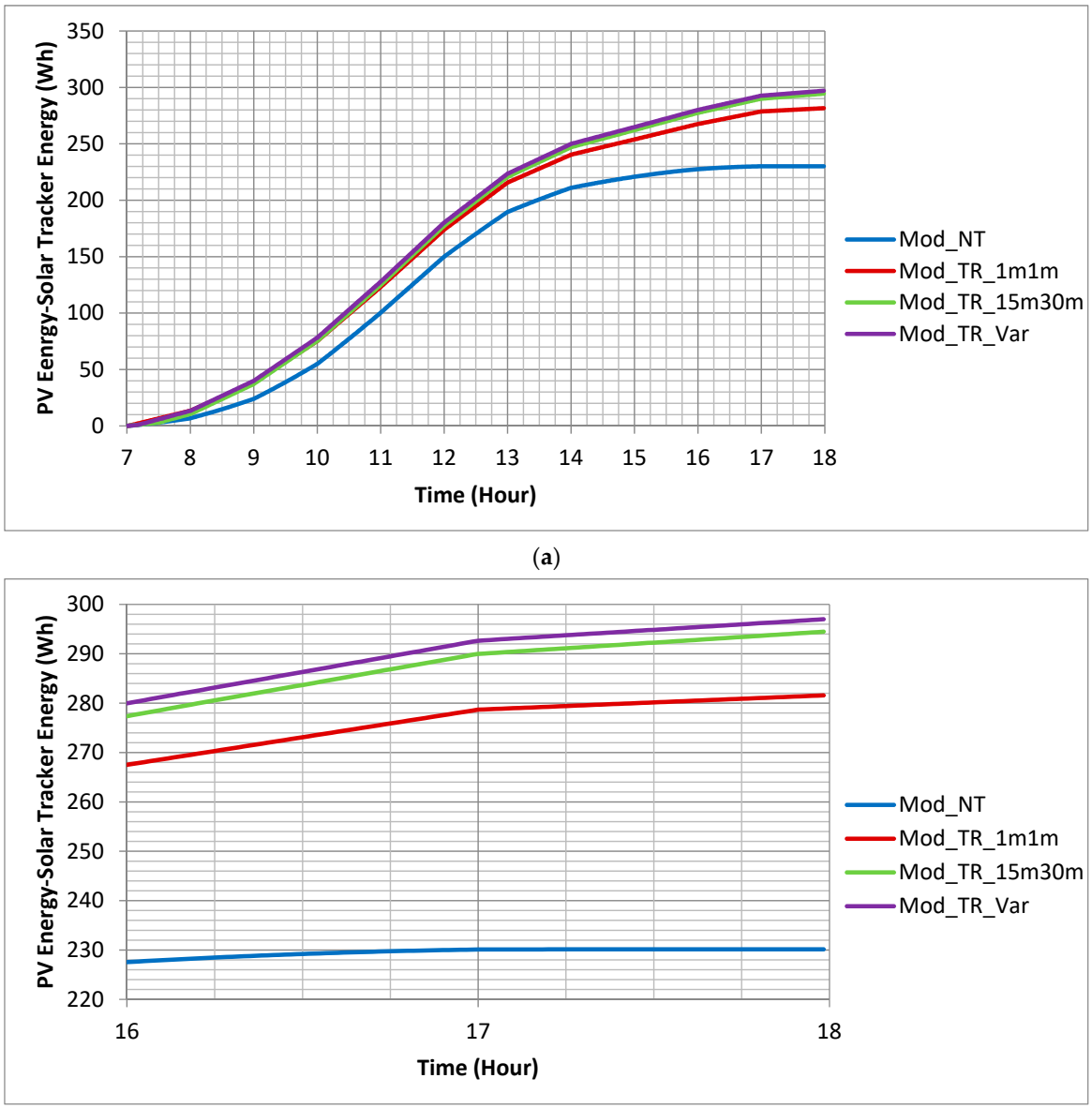

Figure 15. Net energy values produced by models: (**a**) Profiles from 07:00 to 17:59 h; (**b**) Closer look profiles from 16:00 to 17:59 h.

Table 4. Comparison of net energy values produced by models.

Model	PV Energy (Wh)	Tracker Energy (Wh)	Net Energy (Wh)	Increase in Net Energy (%)
Mod_NT	230.1428	0	230.1428	0
Mod_TR_1m1m	299.8875	18.3056	281.5819	22.35
Mod_TR_15m30m	295.3735	0.8889	294.4846	27.96
Mod_TR_Var	298.4803	1.4722	297.0081	29.05

Furthermore, we investigate the effect of the value of solar tracker time interval on the net energy as follows. We compare the seven scenarios, namely: (a) Fixed time interval of 10 min (F_10m); (b) Fixed time interval of 15 min (F_15m); (c) Fixed time interval of 20 min (F_20m); (d) Variable time intervals of 10 min and 15 min (V_10m_15m); (e) Variable time intervals of 10 min and 20 min (V_10m_20m); (f) Variable time intervals of 15 min and 10 min (V_15m_10m); (g) Variable time intervals of 20 min and 10 min (V_20m_10m). Here, F_xm indicates that both the azimuth and elevation trackers move every

x min from 07:00 to 17:59 h. V_xm_ym indicates that both the azimuth and elevation trackers move every x min during the low solar irradiation periods (07:00 to 09:59 h and 14:00 to 17:59 h) and every y min during the high solar irradiation period (10:00 to 13:59 h).

A comparison result of the net energy values produced using the seven scenarios is given in Figure 16. In the case of the fixed time interval, increasing the interval from 10 to 15 min increases the net energy; however, when the time interval is increased to 20 min, the net energy will be reduced. It indicates that there is an optimal time interval that should be properly selected to achieve the maximum net energy.

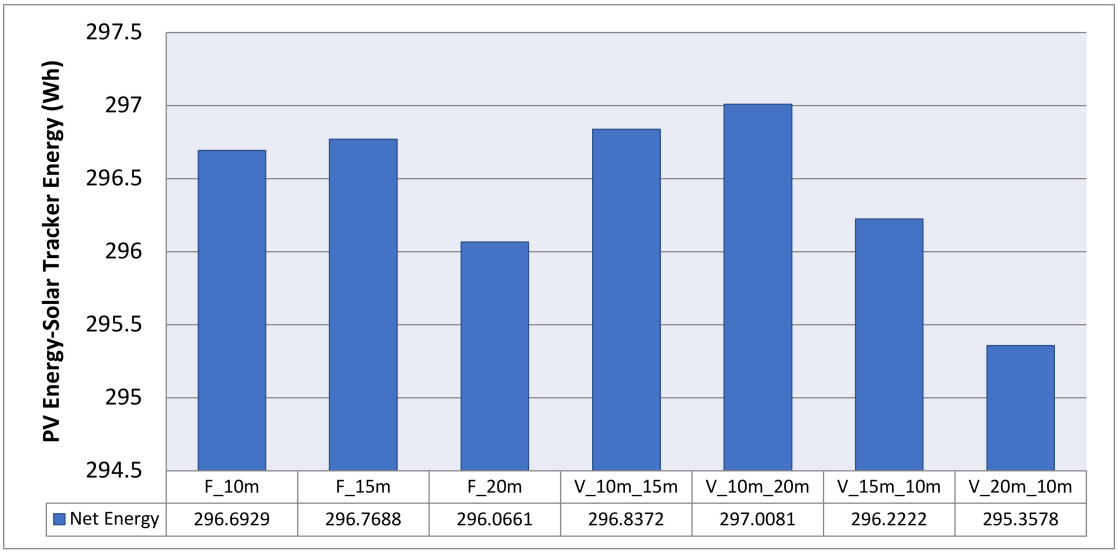

Figure 16. Comparison result of net energy values produced by seven scenarios.

In the case of the variable time intervals, the maximum net energy is achieved by V_10m_20m (as adopted in our proposed method given in Table 1). By comparing the four scenarios of the variable time intervals, we can obtain several findings as follows:

- Comparing V_10m_15m to V_10m_20m, it is obtained that the net energy will be increased when the time interval during a period of high solar irradiation is increased.
- Comparing V_15m_10m to V_20m_10m, it is obtained that the net energy will be decreased when the time interval during a period of low solar irradiation is increased.

From the above findings, it is obtained that increasing the time interval during a period of high solar irradiation yields the opposite effect of doing so during a period of low solar irradiation. It could be analyzed from the fact that increasing the time interval will decrease both the PV energy and the tracker energy, and since the tracker energy is not dependent on the solar irradiation, the effect of increasing the time interval at different solar irradiation levels is determined by the PV energy. By increasing the time interval, the PV energy reduction during the high solar irradiation period is smaller than that during low solar irradiation period. Therefore, prolonging the time interval during a period of high solar irradiation will increase the net energy.

4. Conclusions

The implementation of the discrete model of the PV system on the embedded platform is developed. The PV system employs the MPPT technique and a dual-axis solar tracking system to improve its energy generation. The proposed discrete model is suitable for running a real-time simulation of the PV system, which is an important task in PV system research studies. In addition to the discrete model, a new approach to control the operation time interval of the solar tracker is also developed. The proposed approach uses different time intervals for different periods: those with the high solar

irradiation and low solar irradiation. This approach provides an effective solution to achieve the optimal net energy, which is the subtraction of the PV energy by the consumed solar tracker energy.

In the future, we will extend our discrete model to cover complex models and large PV systems. Furthermore, advanced algorithms for optimizing the net energy will be developed.

Author Contributions: A.S. proposed and implemented the system and wrote the paper; I.B.S. shared the idea about the electrical system. All authors have read and agreed to the published version of the manuscript.

Funding: This work was supported by the Research Grant from Ministry of Research and Technology/National Research and Innovation Agency, Republic of Indonesia (No.: 187/SP2H/LT/DRPM/2020).

Conflicts of Interest: The authors declare no conflict of interest.

References

1. Bendib, B.; Belmili, H.; Krim, F. A survey of the most used MPPT methods: Conventional and advanced algorithms applied for photovoltaic systems. *Renew. Sustain. Energy Rev.* **2015**, *45*, 637–648. [CrossRef]
2. Soetedjo, A.; Lomi, A.; Nakhoda, Y.I.; Krismanto, A.U. Modeling of Maximum Power Point Tracking Controller for Solar Power System. *Telkomnika* **2012**, *10*, 419–430. [CrossRef]
3. Jusoh, A.B.; Mohammed, O.J.E.I.; Sutikno, T. Variable Step Size Perturb and Observe MPPT for PV Solar Applications. *Telkomnika* **2015**, *13*, 1–12. [CrossRef]
4. Soetedjo, A.; Sulistiawati, I.B.; Nakhoda, Y.I. A Modified Step Size Perturb and Observe Maximum Power Point Tracking for PV System. In Proceedings of the 2019 International Conference on Engineering, Science, and Industrial Applications (ICESI), Tokyo, Japan, 22–24 August 2019; pp. 1–6. [CrossRef]
5. Macaulay, J.; Zhou, Z. A Fuzzy Logical-Based Variable Step Size P&O MPPT Algorithm for Photovoltaic System. *Energies* **2018**, *11*, 1340. [CrossRef]
6. Alik, R.; Jusoh, A. Modified Perturb and Observe (P&O) with checking algorithm under various solar irradiation. *Sol. Energy* **2017**, *148*, 128–139. [CrossRef]
7. Killi, M.; Samanta, S. Modified Perturb and Observe MPPT Algorithm for Drift Avoidance in Photovoltaic Systems. *IEEE Trans. Ind. Electron.* **2015**, *62*, 5549–5559. [CrossRef]
8. Putri, R.I.; Wibowo, S.; Rifa'i, M. Maximum power point tracking for photovoltaic using incremental conductance method. *Energy Procedia* **2015**, *68*, 22–30. [CrossRef]
9. Liu, F.; Duan, S.; Liu, F.; Liu, B.; Kang, Y. A Variable Step Size INC MPPT Method for PV Systems. *IEEE Trans. Ind. Electron.* **2008**, *55*, 2622–2628. [CrossRef]
10. Isaloo, B.A.; Amiri, P. Improved Variable Step Size Incremental Conductance MPPT Method with High Convergence Speed for PV Systems. *J. Eng. Sci. Technol.* **2016**, *11*, 516–528.
11. Ambikapathy, A.; Singh, G.; Tiwari, P. Smart Switching Algorithm Between IC and PO Algorithms for Grid-Connected PV System. In *Advances in Smart Grid and Renewable Energy*; Lecture Notes in Electrical Engineering; Springer: Singapore, 2018; Volume 435, pp. 83–92. [CrossRef]
12. Othman, A.M.; El-arini, M.M.M.; Ghitas, A.; Fathy, A. Realworld maximum power point tracking simulation of PV system based on Fuzzy Logic control. *NRIAG J. Astron. Geophys.* **2012**, *1*, 186–194. [CrossRef]
13. Raghuwanshi, S.S.; Khare, V. FLC based MPPT controller for optimal tracking photovoltaic system. In Proceedings of the 2017 International Conference on Information Communication Instrumentation and Control (ICICIC), Indore, India, 17–19 August 2017; pp. 1–6. [CrossRef]
14. Gupta, A.; Kumar, P.; Pachauri, R.K.; Chauhan, Y.K. Performance analysis of neural network and fuzzy logic based MPPT techniques for solar PV systems. In Proceedings of the 2014 6th IEEE Power India International Conference (PIICON), Delhi, India, 5–7 December 2014; pp. 1–6. [CrossRef]
15. Al-Majidi, S.D.; Abbod, M.F.; Al-Raweshidy, H.S. A novel maximum power point tracking technique based on fuzzy logic for photovoltaic systems. *Int. J. Hydrogen Energy* **2018**, *43*, 14158–14171. [CrossRef]
16. Roy, S.K.; Hussain, S.; Bazaz, M.A. Implementation of MPPT technique for solar PV system using ANN. In Proceedings of the 2017 Recent Developments in Control Automation & Power Engineering (RDCAPE), Noida, India, 26–27 October 2017; pp. 338–342. [CrossRef]
17. Racharla, S.; Rajan, K. Solar tracking system—A review. *Int. J. Sustain. Eng.* **2017**, *10*, 72–81. [CrossRef]

18. Zhen, Z.; Zengwei, Z.; Li, S.; Jun, W.; Wuchun, P.; Zhikang, L.; Yunhua, S. The effects of inclined angle modification and diffuse radiation on the sun-tracking photovoltaic system. *IEEE J. Photovolt.* **2017**, *7*, 1410–1415. [CrossRef]
19. Pelaez, S.A.; Deline, C.; Greenberg, P.; Stein, J.S.; Kostuk, R.K. Model and Validation of Single-Axis Tracking With Bifacial PV. *IEEE J. Photovolt.* **2019**, *9*, 715–721. [CrossRef]
20. Katrandzhiev, N.T.; Karnobatev, N.N. Algorithm for Single Axis Solar Tracker. In Proceedings of the 2018 IEEE XXVII International Scientific Conference Electronics—ET, Sozopol, Bulgaria, 13–15 September 2018; pp. 1–4. [CrossRef]
21. Kinsey, G.S.; Partani, M.; Kulkarni, M.; Shetty, B.; Sidhu, R.; Zhang, J. Performance comparison of co-located fixed-tilt and single-axis tracker arrays. In Proceedings of the 2019 IEEE 46th Photovoltaic Specialists Conference (PVSC), Chicago, IL, USA, 16–21 June 2019; pp. 2097–2099. [CrossRef]
22. Tseng, K.; Wang, C.; Lin, G. Effect of the Sun Elevation for Fixed PV System and Single-Axis-Tracking PV System. In Proceedings of the 2019 IEEE 6th International Conference on Industrial Engineering and Applications (ICIEA), Tokyo, Japan, 12–15 April 2019; pp. 805–809. [CrossRef]
23. Hammad, B.K.; Fouad, R.H.; Ashhab, M.S.; Nijmeh, S.D.; Mohsen, M.; Tamimi, A. Adaptive control of solar tracking system. *IET Sci. Meas. Technol.* **2014**, *8*, 426–431. [CrossRef]
24. Flores-Hernandez, D.A.; Palomino-Resendiz, S.I.; Luviano-Juárez, A.; Lozada-Castillo, N.; Gutierrez-Frias, O. A heuristic approach for tracking error and energy consumption minimization in solar tracking systems. *IEEE Access* **2018**, *7*, 2755–52768. [CrossRef]
25. Chowdhury, M.E.H.; Khandakar, A.; Hossain, B.; Abouhasera, R. A low-cost closed-loop solar tracking system based on the sun position algorithm. *J. Sens.* **2019**, *2019*, 1–11. [CrossRef]
26. Alexandru, C. A novel open-loop tracking strategy for photovoltaic systems. *Sci. World J.* **2013**, *2013*, 1–12. [CrossRef]
27. Mustafa, F.I.; Al-Ammri, A.S.; Ahmad, F.F. Direct and indirect sensing two-axis solar tracking system. In Proceedings of the 8th International Renewable Energy Congress (IREC), Amman, Jordan, 21–23 March 2017; pp. 1–4. [CrossRef]
28. Fathabadi, H. Novel online sensorless dual-axis Sun tracker. *IEEE/ASME Trans. Mechatron.* **2017**, *22*, 321–328. [CrossRef]
29. Ikhwan, M.; Imron, C. Model predictive control on dual axis solar tracker using Matlab/Simulink simulation. In Proceedings of the 2018 International Conference on Information and Communications Technology (ICOIACT), Yogyakarta, Indonesia, 6–7 March 2018; pp. 784–788. [CrossRef]
30. Ahmad, S.; Shafie, S.; Kadir, Z. Power Feasibility of a Low Power Consumption Solar Tracker. *Procedia Environ. Sci.* **2013**, *17*, 494–502. [CrossRef]
31. Soetedjo, A.; Sulistiawati, I.B.; Nakhoda, Y.I. Integration of Solar Tracker and Maximum Power Point Tracking for Improving Photovoltaic (PV) System Efficiency. *Int. J. Innov. Comput. Inf. Control* **2020**, *16*, 429–443. [CrossRef]
32. Ferdaus, R.A.; Mohammed, M.A.; Rahman, S.; Salehin, S.; Mannan, M.A. Energy Efficient Hybrid Dual Axis Solar Tracking System. *J. Renew. Energy* **2014**, *2014*, 1–12. [CrossRef]
33. Ando, B.; Baglio, S.; Pistorio, A.; Tina, G.M.; Ventura, C. Sentinella: Smart Monitoring of Photovoltaic Systems at Panel Level. *IEEE Trans. Instrum. Meas.* **2015**, *64*, 2188–2199. [CrossRef]
34. Aghenta, L.O.; Iqbal, M.T. Development of an IoT Based Open Source SCADA System for PV System Monitoring. In Proceedings of the 2019 IEEE Canadian Conference of Electrical and Computer Engineering (CCECE), Edmonton, AB, Canada, 5–8 May 2019; pp. 1–4. [CrossRef]
35. Pereira, R.I.S.; Juca, S.C.S.; Carvalho, P.C.M. IoT embedded systems network and sensors signal conditioning applied to decentralized photovoltaic plants. *Measurement* **2019**, *142*, 195–212. [CrossRef]
36. Priyadarshi, S.; Bhaduri, S.; Shiradkar, N. IoT Based, Inexpensive System for Large Scale, Wireless, Remote Temperature Monitoring of Photovoltaic Modules. In Proceedings of the 2018 IEEE 7th World Conference on Photovoltaic Energy Conversion (WCPEC) (A Joint Conference of 45th IEEE PVSC, 28th PVSEC & 34th EU PVSEC), Waikoloa Village, HI, USA, 10–15 June 2018; pp. 0749–0752. [CrossRef]
37. Shapsough, S.; Takrouri, M.; Dhaouadi, R.; Zualkernan, I. An IoT-based remote IV tracing system for analysis of city-wide solar power facilities. *Sustain. Cities Soc.* **2020**, *57*. [CrossRef]

38. Rouibah, N.; Barazane, L.; Mellit, A.; Hajji, B.; Rabhi, A. A low-cost monitoring system for maximum power point of a photovoltaic system using IoT technique. In Proceedings of the 2019 International Conference on Wireless Technologies, Embedded and Intelligent Systems (WITS), Fez, Morocco, 3–4 April 2019; pp. 1–5. [CrossRef]
39. Lopez-Vargas, A.; Fuentes, M.; Vivar, M. IoT Application for Real-Time Monitoring of Solar Home Systems Based on Arduino With 3G Connectivity. *IEEE Sens. J.* **2019**, *19*, 679–691. [CrossRef]
40. Paredes-Parra, J.M.; García-Sánchez, A.J.; Mateo-Aroca, A.; Molina-García, A. An Alternative Internet-of-Things Solution Based on LoRa for PV Power Plants: Data Monitoring and Management. *Energies* **2019**, *12*, 881. [CrossRef]
41. Lin, Y.F.; Lin, P.J.; Zhou, H.F.; Chen, Z.C.; Wu, L.J.; Cheng, S.Y.; Su, F.P. On-line monitoring system of PV array based on internet of things technology. *IOP Conf. Ser. Earth Environ. Sci.* **2017**, *93*, 1–12. [CrossRef]
42. Prasanna, J.L.; Lavanya, D.; Kumar, T.A. Condition monitoring of a virtual solar system using IoT. In Proceedings of the 2017 2nd International Conference on Communication and Electronics Systems (ICCES), Coimbatore, India, 19–20 October 2017; pp. 286–290. [CrossRef]
43. Lopez-Vargas, A.; Fuentes, M.; Vivar, M. On the application of IoT for real-time monitoring of small stand-alone PV systems: Results from a new smart datalogger. In Proceedings of the 2018 IEEE 7th World Conference on Photovoltaic Energy Conversion (WCPEC) (A Joint Conference of 45th IEEE PVSC, 28th PVSEC & 34th EU PVSEC), Waikoloa Village, HI, USA, 10–15 June 2018; pp. 605–607. [CrossRef]
44. Jagoo, Z. *Tracking Solar Concentrators–A Low Budget Solution*; Springer: Heidelberg, Germany, 2013. [CrossRef]
45. Computing Planetary Positions—A Tutorial with Worked Examples. Available online: http://stjarnhimlen.se/comp/tutorial.html#5 (accessed on 1 May 2020).
46. Converting RA and DEC to ALT and AZ. Available online: http://www.stargazing.net/kepler/altaz.html (accessed on 1 May 2020).
47. File Exchange: Vectorized Solar Azimuth and Elevation Estimation. Available online: https://www.mathworks.com/matlabcentral/fileexchange/23051-vectorized-solar-azimuth-and-elevation-estimation (accessed on 1 May 2020).
48. Nguyen, X.H.; Nguyen, M.P. Mathematical modeling of photovoltaic cell/module/arrays with tags in Matlab/Simulink. *Environ. Syst. Res.* **2015**, *4*, 1–13. [CrossRef]
49. Selmi, T.; Bouzguenda, M.; Gastli, A.; Masmoudi, A. MATLAB/Simulink Based Modelling of Solar Photovoltaic Cell. *Int. J. Renew. Energy Res.* **2012**, *2*, 213–218.
50. Tsai, H.L.; Ci-Siang, T.; Yi-Jie, S. Development of generalized photovoltaic model using MATLAB/SIMULINK. In Proceedings of the World Congress on Engineering and Computer Science (WCECS 2008), San Francisco, CA, USA, 22–24 October 2008; p. 2173.
51. Introduction to Power Electronics. Available online: https://ecee.colorado.edu/~{}ecen5797/ (accessed on 1 May 2020).
52. Wemos D1 Mini Pro. Available online: https://docs.wemos.cc/en/latest/d1/d1_mini_pro.html (accessed on 10 May 2020).